Defect-induced electronic smectic state at the surface of nematic materials

Aritra Lahiri, Avraham Klein, and Rafael M. Fernandes

Phys. Rev. B **106**, L140503 — Published 10 October 2022

DOI: 10.1103/PhysRevB.106.L140503

Defect-induced electronic smectic state at the surface of nematic materials

Aritra Lahiri,[1,*] Avraham Klein,[2] and Rafael M. Fernandes[1,†]

[1] *School of Physics and Astronomy, University of Minnesota, Minneapolis, Minnesota 55455, USA*
[2] *Physics Department, Ariel University, Ariel 40700, Israel*

(Dated: September 22, 2022)

Due to the intertwining between electronic nematic and elastic degrees of freedom, lattice defects and structural inhomogeneities commonly found in crystals can have a significant impact on the electronic properties of nematic materials. Here, we show that defects commonly present at the surface of crystals generally shift the wave-vector of the nematic instability to a non-zero value, resulting in an incommensurate electronic smectic phase. Such a smectic state onsets above the bulk nematic transition temperature and is localized near the surface of the sample. We argue that this effect may explain not only recent observations of a modulated nematic phase in iron-based superconductors, but also several previous puzzling experiments that reported signatures consistent with nematic order before the onset of a bulk structural distortion.

Electronic nematicity has been observed in a wide range of systems, including high-T_c superconductors [1–3], heavy-fermion materials [4–6], topological superconductors [7, 8], cold atoms [9], and twisted moiré devices [10, 11]. Among those, iron-based superconductors (FeSC) have provided unique insight into this quantum electronic state due to the nearly-universal and unambiguous presence of nematic order and nematic fluctuations in their phase diagrams [3, 12–16]. Despite significant progress, essential questions remain unresolved, related not only to the microscopic mechanisms of nematicity, but also to its general phenomenology [17]. For instance, since early studies of FeSC, various probes in nominally unstrained samples have reported signatures consistent with nematicity above the nematic transition temperature $T_{\rm nem}$ established by thermodynamic probes [18–29]. More recently, experiments have found evidence for a spatially-modulated nematic phase – i.e. an electronic smectic phase [30–33].

The probes used in many of these experiments are particularly sensitive to the surface, e.g. angle-resolved photo-emission spectroscopy (ARPES) [25–27], scanning tunneling microscopy (STM) [21, 30–32], spatially resolved photomodulation [19], and photo-emission electron microscopy (PEEM) [33]. Moreover, the onset of these interesting phenomena does not usually show typical phase-transition signatures in thermodynamic quantities, such as specific heat [34] and elasto-resistance [3]. This suggests that both effects – nematic manifestations above $T_{\rm nem}$ and modulated nematic order – may signal a surface nematic transition at higher temperatures than the bulk one [19], reminiscent of the so-called extraordinary transition [35]. The key question is whether a surface nematic transition is particular to some FeSC compounds or a more general phenomenological property of nematic compounds.

While a purely electronic mechanism was previously invoked to explain surface nematicity [36], in this Letter we focus on the role of the elastic degrees of freedom. The nemato-elastic coupling g is known to significantly impact the nematic state, particularly in FeSC [15, 16, 37–42]. For instance, coupling to elastic fluctuations (acoustic phonons) renders the nematic transition mean-field like [41, 43–46], whereas intrinsic random strain fosters behaviors associated with the random-field Ising-model [47–49]. Here, we show that defects commonly found in the surfaces of crystals, such as steps separating terrace domains, promote an electronic smectic state localized near the surface and that onsets at a temperature $T_{\rm smc} > T_{\rm nem}$ (see Fig. **1**). The smectic state survives down to a temperature $T_{\rm smc-nem}$, which decreases as the sample thickness is reduced, at which point a homogeneous nematic phase takes over. Our results establish a hitherto unexplored facet of electronic nematic phases in elastic media, which we argue can explain the intriguing observation of Ref. [33] of a mesoscopic nematic wave in FeSC.

To understand why defects induce a surface transition, note that elastic fluctuations increase the nematic transition temperature $T_{\rm nem}$ from its bare purely-electronic value $T_{\rm nem}^{(0)}$. In a clean system, some of the elastic modes are expected to be frozen near the surface, resulting in $T_{\rm nem}^{(\rm surface)} < T_{\rm nem}$ [50]. However, the fact that the exposed surface is more disordered than the bulk changes this picture dramatically. To see this, consider a random distribution of defects, such as vacancies and dislocations, on the surface of a crystal whose bulk is clean. Defects locally induce large strains that decay slowly with distance [51]. Since they are concentrated at the surface, they rapidly screen each other as one moves deeper into the bulk. However, near the surface, they do not screen efficiently, causing not only an enhancement of $T_{\rm nem}$ at the surface, but also creating a "speckle" pattern in the nematic fluctuation spectrum, with typical spot size set by the algebraic strain correlations rather than by the defect density. This disorder-induced pattern imposes a preferred wavelength for the condensation of the nematic order parameter, driving the formation of an electronic smectic state.

To derive these results, we solve a Ginzburg-Landau

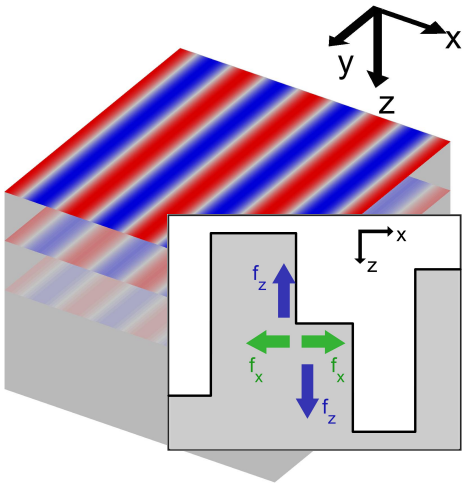

Figure 1. (color online) Schematic illustration of the surface smectic state, shown here as a modulated nematic order parameter that quickly decays in the bulk of the sample (gray). Red (blue) regions denote a B_{1g} nematic order parameter that selects the x (y) axis of a tetragonal crystal. The inset illustrates the dipolar forces induced by a surface step. It also presents a cross-section of the sample (gray) with aligned steps of random heights/strengths oriented parallel to the $y-$axis.

model of a generic nematic order parameter coupled to elastic strain induced by simple types of surface quenched disorder, such as steps and anisotropic point defects. We find that the defect distribution induces a non-local effective potential for the nematic order parameter. After averaging over defect realizations, the minimum of the resulting nematic free energy appears at a higher temperature $T_{\rm smc} = T_{\rm nem} + \Delta T_{\rm smc}$ (with $\Delta T_{\rm smc} > 0$) and at a non-zero wave-vector $q_{\rm smc}$, resulting in an electronic smectic phase. In terms of the disorder strength σ^2, we find

$$q_{\rm smc} \propto g^2\sigma^2, \quad \Delta T_{\rm smc} \propto q_{\rm smc}^2, \tag{1}$$

The smectic order parameter is inhomogeneous and localized at the the surface, decaying exponentially into the bulk with a penetration depth $\propto 1/q_{\rm smc}$. Eventually, below $T_{\rm smc-nem}$, which is lower than the bulk nematic transition temperature $T_{\rm nem}$, the smectic solution becomes unfavorable and the uniform $q = 0$ nematic state is established throughout the sample.

Surface step disorder and induced strain.– To elucidate our results, we consider an Ising-nematic order parameter η that breaks the equivalence between the x and y directions of a crystal (i.e. it transforms as the B_{1g} irreducible representation of the tetragonal group). In the presence of strain, the nematic action is given by:

$$S = \int_{\boldsymbol{r}} \left[\left(r_0 \frac{T - T_{\rm nem}}{2T_{\rm nem}^{(0)}} \right) \eta_{\boldsymbol{r}}^2 + \frac{b_\mu}{2} (\partial_\mu \eta_{\boldsymbol{r}})^2 - g \varepsilon_{\boldsymbol{r}}^{B_{1g}} \eta_{\boldsymbol{r}} + \frac{u_\eta}{4} \eta_{\boldsymbol{r}}^4 \right] \tag{2}$$

where repeated indices are implicitly summed; $b_x = b_y = b_\parallel$ and b_z are the nematic stiffness coefficients; $u_\eta > 0$ is the quartic coefficient; r_0 is of the order of the Fermi energy (action has dimensions of energy); $\varepsilon^{B_{1g}} \equiv (\varepsilon_{xx} - \varepsilon_{yy})/\sqrt{2}$ is the B_{1g} shear strain, which acts as a conjugate field to the nematic order parameter; and $T_{\rm nem}^{(0)}, T_{\rm nem}$ are the nematic transition temperatures without and with the enhancement from elastic fluctuations. For a clean unstrained crystal, $\varepsilon_{\boldsymbol{r}}^{B_{1g}}$ is only present as a fluctuating field whose properties are determined by the crystal's elastic constants. However, for a crystal with quenched disorder, a static slow-decaying strain $\varepsilon_{\boldsymbol{r}}^{B_{1g}}$ is generated by the various types of defects. In both cases, an effective nematic potential emerges in the action due to either thermal fluctuations or average over disorder configurations. While the former scenario has been widely studied [43–46], the latter has received much less attention [52, 53].

A crystal with an exposed surface can be modeled by an isotropic elastic half-space ($z \geq 0$) with Young's modulus E and Poisson ratio ν. Each type of surface defect generates a characteristic dipolar local force, which in turn can be used to calculate $\varepsilon_{\boldsymbol{r}}^{B_{1g}}$ via standard methods [54–60]. Here, we consider idealized infinite step defects parallel to the $y-$axis, as shown in Fig. 1 (we consider point defects in the Supplementary material (SM) [61]). A single step at $x = x'$ is parametrized by the force density $f_\mu = h_\mu[\partial_x \delta(x - x')]\delta(z)$, where $\delta(z)$ is the Dirac delta function, the force h_μ characterizes the strength of the defect, and $\mu = x, z$. For simplicity, we consider steps that create forces along the $z-$axis only, i.e. $h_x = 0$ and $h_z \neq 0$. The lattice displacement created by a single step is given by $u_\mu = h_\nu \partial_x G_{\mu\nu}(x - x', z)$, where $G_{\mu\nu}$ is the Green's function for an infinite line-force along the $y-$axis in half-space [51]. The B_{1g} strain $\varepsilon_{\boldsymbol{r}-\boldsymbol{r}'}^{B_{1g}}$ generated by a single defect is [51]

$$\varepsilon_{\boldsymbol{r}-\boldsymbol{r}'}^{B_{1g}} = \frac{-4(1+\nu)h_z}{\sqrt{2}\pi E} \left[\frac{(\nu - 1)\,\delta x^3 z + (\nu + 1)\,\delta x\, z^3}{\left(\delta x^2 + z^2\right)^3} \right], \tag{3}$$

where $\delta x = x - x'$. A distribution of such steps at random positions $x = x_j$ and with random strength $h_{z,j}$ results in the net B_{1g} strain $\varepsilon_{\boldsymbol{r}}^{B_{1g}} = \sum_j h_j \partial_x^2 G_{xz}(x - x', z - 0) \equiv \sum_j h_j \bar{\varepsilon}_{\boldsymbol{r}-\boldsymbol{r}_j}^{B_{1g}}$. The nematic action (2) for the finite crystal with dimensions $L_x = L_y = L_\parallel$ and $L_z = L \ll L_\parallel$ becomes:

$$\begin{aligned} S = & L_\parallel \int_{-\frac{L_\parallel}{2}}^{\frac{L_\parallel}{2}} dx \int_0^L dz \left[\left(r_0 \frac{T - T_{\rm nem}}{2T_{\rm nem}^{(0)}} \right) \eta_{x,z}^2 + \frac{b_\parallel}{2} (\partial_x \eta_{x,z})^2 \right. \\ & \left. + \frac{b}{2} (\partial_z \eta_{x,z})^2 + \frac{u_\eta}{4} \eta_{x,z}^4 - g \int_{-\frac{L_\parallel}{2}}^{\frac{L_\parallel}{2}} dx' \rho_{x'} \bar{\varepsilon}_{x-x',z}^{B_{1g}} \eta_{x,z} \right], \end{aligned} \tag{4}$$

where we defined $\rho_x = \sum_j h_j \delta(x - x_j)$.

Effective nematic potential and smectic state.— For a random distribution of steps, $\langle h_j h_{j'}\rangle = \sigma^2\delta_{j,j'}$, the step density ρ_x follows a Gaussian distribution with variance $\sigma^2(N_{\rm step}/L_\parallel)(a_\parallel/L_\xi)$, where $N_{\rm step}$ is the number of steps, $a_\parallel$ is the in-plane lattice constant, and L_ξ is a length scale larger than $a_\parallel$ but smaller than the nematic correlation length. Integrating out the step density in Eq. (4) (equivalent to the standard procedure of averaging over quenched disorder [62–68]) generates a new quadratic term in the nematic action:

$$S_d = L_\parallel^2 \int_0^L dz\, dz' \sum_{q_x} V_{q_x,z,z'}\eta^*_{q_x,z}\eta_{q_x,z'} \tag{5}$$

with an effective potential experienced by the nematic order parameter

$$\begin{aligned} V_{q_x,z,z'} = &-\frac{(g\sigma)^2\beta}{2}\, e^{-|q_x|(|z|+|z'|)} \\ &\times q_x^2[|q_x||z|+2\nu-1][|q_x||z'|+2\nu-1]. \end{aligned} \tag{6}$$

Here, $\beta = [(1+\nu)/(\sqrt{2}E)]^2 N_{\rm step}(L_\xi/a_\parallel)$ and $\eta_{q_x,z} = (1/L_\parallel)\int_x \eta_{x,z}e^{-iq_x x}$. The potential $V_{q_x,z,z'}$ is non-local, depending on both z and z'. Moreover, it vanishes quadratically as $q_x \to 0$ and exponentially as $z,\, z' \to \infty$ or $q_x \to \infty$. Thus, the potential has a negative-valued minimum at a non-zero q_x and is significant only near the surface. These features are a consequence of the algebraic decay of the strain fields generated by defects, rather than the type of defects (see SM [61]).

While the defect-generated potential in Eq. (6) is minimized by $q_x \neq 0$, the nematic stiffness term $b_\parallel q_x^2$ in Eq. (4) favors a uniform $q_x = 0$ state. This competition causes the nematic instability to take place at a nonzero wave-vector q_x, resulting in an electronic smectic state. This effect is restricted to the vicinity of the surface due to the exponential suppression of $V_{q_x,z,z'}$ with $|z|$. This can be more clearly seen by an approximate analytical solution of the problem. Re-expressing $V_{q_x,z,z'}$ in terms of $\bar{z} = (z+z')/2$ and $\delta z = z - z'$, $V_{q_x,\bar{z},\delta z}$ is peaked at $\bar{z} \sim 1/|q_x|$ and $\delta z = 0$. Assuming that $\eta_{q_x,z}$ varies slowly near the surface over a depth $L_s \sim 1/|q_x|$, before eventually decaying exponentially away from the surface, the action (5) becomes:

$$\begin{aligned} S_d =& L_\parallel^2 \int_{\bar{z}=0}^{L}\int_{\delta z=-\frac{L_s}{2}}^{\frac{L_s}{2}} \sum_{q_x} V_{q_x,\bar{z},\delta z}|\eta_{q_x,0}|^2, \\ \approx& -L_\parallel^2 L_s \sum_{q_x} \frac{(g\sigma)^2\beta\left[(\nu-\frac{1}{2})^2+\nu^2\right]}{2}\,|q_x||\eta_{q_x,0}|^2. \end{aligned} \tag{7}$$

In the regime of vanishing z-component stiffness $b \to 0$, the quadratic part of the action (4), $S^{(2)}$, is given by:

$$S^{(2)} \approx L_\parallel^2 L_s \sum_{q_x}\left[\left(r_0\frac{T-T_{\rm nem}}{2T^{(0)}_{\rm nem}}\right) + \frac{b_\parallel q_x^2}{2}\right]|\eta_{q_x,0}|^2 \tag{8}$$

Minimizing the full action $S_d + S^{(2)}$ with respect to q_x gives a finite smectic wave-vector $q_{\rm smc} = (g\sigma)^2\beta\left[(\nu-\frac{1}{2})^2+\nu^2\right]/2b_\parallel$ and an enhanced smectic transition temperature $T_{\rm smc} = T_{\rm nem} + (T^{(0)}_{\rm nem}/r_0)b_\parallel q^2_{\rm smc}$, consistent with Eq. (1). The actual spatial profile of $\eta_{x,z}$ and the precise $q_{\rm smc}$ and $T_{\rm smc}$ can be obtained by solving the saddle-point equation in real space,

$$\begin{aligned} &\left[r_0\frac{T-T_{\rm nem}}{T^{(0)}_{\rm nem}} - b\partial_z^2 - b_\parallel\partial_x^2\right]\eta_{x,z} + u_\eta\eta^3_{x,z} \\ &\quad + \frac{1}{L_\parallel}\int_0^L dz' \int_{-\frac{L_\parallel}{2}}^{\frac{L_\parallel}{2}} dx'\, V_{x-x',z,z'}\eta_{x',z'} = 0 \end{aligned} \tag{9}$$

where $V_{\delta x,z,z'}$ is the inverse Fourier transform of $V_{q_x,z,z'}$ (see SM [61]), whose asymptotic behavior is:

$$V_{\delta x,z,z'} \sim \begin{cases} -(z+z')^{-3} & ,\ |\delta x| \ll z, z' \\ +(z+z')(\delta x)^{-4} & ,\ |\delta x| \gg z, z' \end{cases}. \tag{10}$$

Therefore, as a function of $\delta x/(z+z')$, $V_{\delta x,z,z'}$ has a negative central trough at $\delta x = 0$, crosses zero at $\delta x \sim z+z'$, and then remains positive as it decays algebraically. The sign change in real-space means that the effective potential favors an oscillatory η_x solution.

The numerical solution of Eq. (9), shown in Fig. **2**(a), confirms the main results of our analytical approximation. The quartic term of the nematic action (4) stabilizes a single smectic wave-vector over the entire temperature range $T_{\rm smc-nem} < T < T_{\rm smc}$, as it acts as a repulsive biquadratic interaction $u_\eta|\eta_{q_x}|^2|\eta_{q'_x\neq q_x}|^2$ between states with different wave-vectors. Consequently, only the smectic wave-vector corresponding to the highest critical temperature develops. For the same reason, in a fully 3D crystal with $L \gg 1/q_{\rm smc}$, the uniform bulk nematic phase is preferred for $T < T_{\rm nem}$, as its free-energy gain scales extensively with the system size. However, for smaller values of L comparable to $1/q_{\rm smc}$, the smectic free-energy can compete with the bulk nematic one. Consequently, the smectic-nematic transition is pushed to a lower temperature $T_{\text{smc-nem}} < T_{\rm nem}$, which decreases with decreasing sample thickness. Figs. **2**(b)-(c) show the corresponding profile of $\eta_{q_x,z}$ in momentum space, highlighting the change in wave-vector above and below $T_{\rm smc-nem}$.

The temperature dependence of the uniform nematic and smectic order parameters is shown in Fig. **3**(a). The continuous onset of surface smectic order is evident, eventually dropping discontinuously to zero, concomitant to the onset of uniform nematic order. Fig. **3**(b) shows the numerically obtained phase diagram as a function of increasing defect disorder strength σ^2.

Discussion.— The mechanism unveiled in this work for the emergence of a surface electronic smectic state above the onset of bulk electronic nematicity is rather general, as it relies solely on the existence of defects commonly observed at crystal surfaces. While here we focused on

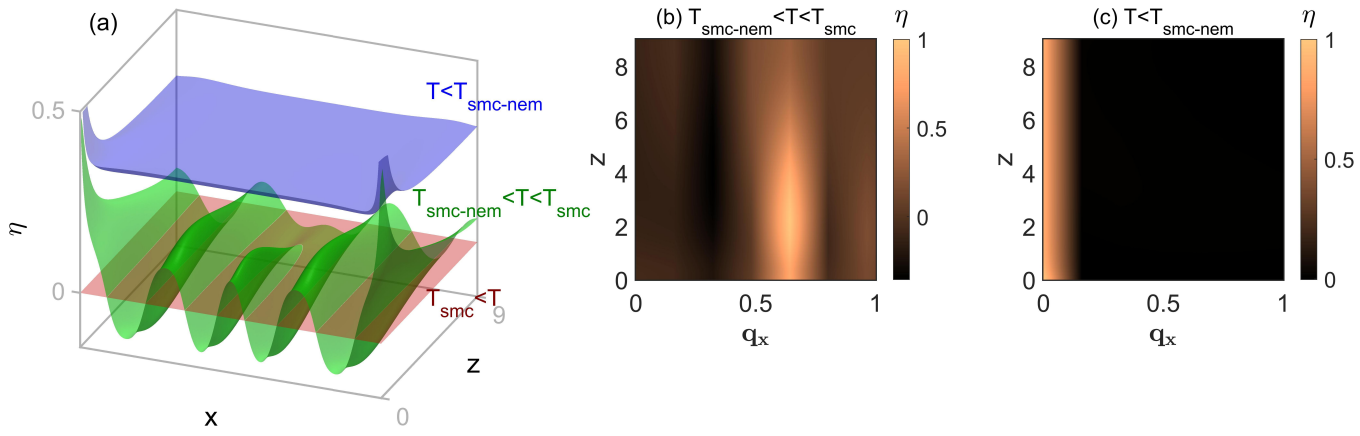

Figure 2. (color online) (a) Spatial profile of the nematic order parameter $\eta_{x,z}$ for three representative temperatures, obtained from the numerical solution of the saddle-point equation (9). For $T > T_{\rm smc}$, the nematic order parameter is effectively zero everywhere. As temperature is lowered towards $T_{\rm smc-nem} < T < T_{\rm smc}$, $\eta_{x,z}$ displays a sinusoidal x-dependence characterized by a single smectic wave-vector $q_{\rm smc}$ [panel (b)]. Below the bulk nematic transition $T < T_{\rm smc-nem}$, a uniform nematic state emerges with zero wave-vector [panel (c)]. The enhancement of $\eta_{x,z}$ at the corners is an artifact of the boundary conditions. The profile of the nematic order parameter $\eta_{q_x,z}$ in Fourier space is shown in panels (b) (for $T_{\rm smc-nem} < T < T_{\rm smc}$) and (c) (for $T < T_{\rm smc-nem}$). The parameters used are (in arbitrary units): $r_0 = 1$, $b = 0.5$, $b_\parallel = 0.25$, $\nu = 0.495$, $L_\parallel = 44$, $L = 9$, $(g\sigma)^2\beta/2 = 1$, and $u_\eta = 5$. In panels (b) and (c), the nematic fields were normalized.

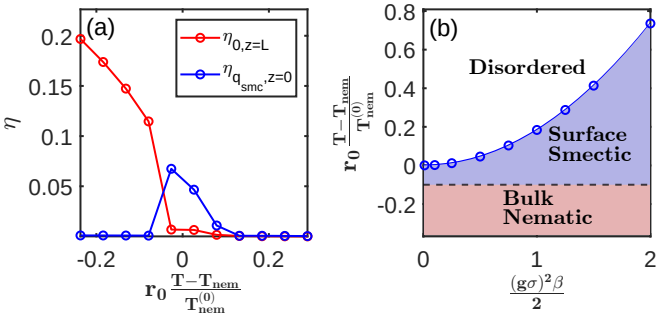

Figure 3. (a) Temperature dependence of the uniform nematic (red, approximated by $\eta_{q_x=0,z=L}$) and surface smectic (blue, approximated by $\eta_{q_x=q_{\rm smc}\approx 0.57,z=0}$) order parameters, numerically obtained by solving Eq. (9) (same parameters as Fig.**2**). (b) Phase diagram as a function of the effective disorder strength $\frac{(g\sigma)^2\beta}{2}$ and the reduced temperature. The smectic critical temperature (blue circles), found to vary quadratically with $\frac{(g\sigma)^2\beta}{2}$, was obtained from the linearized saddle-point equation (9) in momentum space (see SM [61]). Due to the finite sample thickness, the bulk nematic phase onsets at $T = T_{\rm smc-nem} < T_{\rm nem}$.

steps, other defects with nonzero dipolar elastic moments are expected to promote a similar behavior, since they also generate algebraically-decaying strain fields that are poorly screened at the surface (see SM [61]) [69, 70]. Our result unearths yet another aspect of the rich phenomenology of electronic nematicity caused by the coupling to the elastic degrees of freedom.

The impact of the effect we found on a given nematic system depends on the disorder strength σ and on the nemato-elastic coupling g, as shown in the phase diagram of Fig. **3**(b). FeSC stand out as compounds with strongly coupled nematic and elastic degrees of freedom, as manifested by, e.g., the large orthorhombic distortion seen in the nematic phase [71]. In contrast, in other tetragonal correlated systems that display nematic tendencies, such as Hg-based cuprates [72] and heavy-fermion systems [5, 6], a lattice distortion is difficult to be resolved experimentally. The potentially large period $2\pi/q_{\rm smc}$ of the smectic state may explain why certain surface-sensitive probes, such as ARPES and STM, observe signatures consistent with nematic order above the temperature where a bulk orthorhombic distortion onsets. Among the various experimental findings that have indicated the existence of a smectic phase in FeSC [30–33], the PEEM data reported in Ref. [33] provides the most straightforward platform to perform comparisons with our theory and extract relevant physical estimates. That work found a sinusoidal modulation of the nematic order parameter with a long and material-dependent period. Moreover, when Fourier-transformed to momentum space (see the SM [61]), the PEEM data, available in [73], displays a distinctive speckle pattern corresponding to a spot of size $q_{\rm smc}$, reminiscent of our theoretically calculated nematic potential $V_{q_x,z,z'}$. As shown in detail in the SM [61], combining the experimental results of Ref. [33] with our theoretical model, we find two interesting results: (i) The size of a typical region of parallel stripes, observed in that work, is small enough that a homogeneous nematic phase may not be stabilized at $T_{\rm nem}$. (ii) The characteristic energy scale per defect is of the order $E_d \sim 100\mu$eV. This scale is much smaller than both the Fermi energy and the bulk nematic orbital order energy splitting observed in FeSe. These results highlight that

the smectic order is not the result of a particular defect distribution with fine-tuned disorder strength, but of the subtle effects of the long-range strain generated by the defect distribution.

We acknowledge fruitful discussions with B. Davidovitch, D. Pelc, M. Greven, and J. Schmalian. This work was supported by the U. S. Department of Energy, Office of Science, Basic Energy Sciences, Materials Sciences and Engineering Division, under Award No. DE-SC0020045 (R.M.F.). A.K. and R.M.F. acknowledge the hospitality of KITP at UCSB, where part of the work was conducted. The research at KITP is supported by the National Science Foundation under Grant No. NSF PHY-1748958.

* Present address: Theoretical Physics 4, University of Würzburg, 97074 Würzburg, Germany
† rfernand@umn.edu

[1] E. Fradkin, S. A. Kivelson, M. J. Lawler, J. P. Eisenstein, and A. P. Mackenzie, Annual Review of Condensed Matter Physics **1**, 153 (2010).
[2] M. J. Lawler, K. Fujita, J. Lee, A. R. Schmidt, Y. Kohsaka, C. K. Kim, H. Eisaki, S. Uchida, J. C. Davis, J. P. Sethna, et al., Nature **466**, 347 (2010).
[3] J.-H. Chu, H.-H. Kuo, J. G. Analytis, and I. R. Fisher, Science **337**, 710 (2012).
[4] R. Okazaki, T. Shibauchi, H. J. Shi, Y. Haga, T. D. Matsuda, E. Yamamoto, Y. Onuki, H. Ikeda, and Y. Matsuda, Science **331**, 439 (2011).
[5] F. Ronning, T. Helm, K. R. Shirer, M. D. Bachmann, L. Balicas, M. K. Chan, B. J. Ramshaw, R. D. McDonald, F. F. Balakirev, M. Jaime, et al., Nature **548**, 313 (2017).
[6] S. Seo, X. Wang, S. M. Thomas, M. C. Rahn, D. Carmo, F. Ronning, E. D. Bauer, R. D. dos Reis, M. Janoschek, J. D. Thompson, et al., Phys. Rev. X **10**, 011035 (2020).
[7] M. Hecker and J. Schmalian, npj Quantum Materials **3**, 26 (2018).
[8] C.-w. Cho, J. Shen, J. Lyu, O. Atanov, Q. Chen, S. H. Lee, Y. S. Hor, D. J. Gawryluk, E. Pomjakushina, M. Bartkowiak, et al., Nature Communications **11**, 3056 (2020), ISSN 2041-1723.
[9] S. Jin, W. Zhang, X. Guo, X. Chen, X. Zhou, and X. Li, Phys. Rev. Lett. **126**, 035301 (2021).
[10] Y. Cao, D. Rodan-Legrain, J. M. Park, N. F. Q. Yuan, K. Watanabe, T. Taniguchi, R. M. Fernandes, L. Fu, and P. Jarillo-Herrero, Science **372**, 264 (2021).
[11] C. Rubio-Verdú, S. Turkel, L. Song, L. Klebl, R. Samajdar, M. S. Scheurer, J. W. F. Venderbos, K. Watanabe, T. Taniguchi, H. Ochoa, et al., ArXiv:2009.11645 (2020).
[12] J.-H. Chu, J. G. Analytis, K. De Greve, P. L. McMahon, Z. Islam, Y. Yamamoto, and I. R. Fisher, Science **329**, 824 (2010).
[13] T.-M. Chuang, M. P. Allan, J. Lee, Y. Xie, N. Ni, S. L. Bud'ko, G. S. Boebinger, P. C. Canfield, and J. C. Davis, Science **327**, 181 (2010).
[14] R. M. Fernandes and J. Schmalian, Superconductor Science and Technology **25**, 084005 (2012).
[15] A. E. Böhmer and C. Meingast, Comptes Rendus Physique **17**, 90 (2016).
[16] Y. Gallais and I. Paul, Comptes Rendus Physique **17**, 113 (2016).
[17] R. M. Fernandes, A. V. Chubukov, and J. Schmalian, Nature Physics **10**, 97 (2014).
[18] S. Kasahara, H. J. Shi, K. Hashimoto, S. Tonegawa, Y. Mizukami, T. Shibauchi, K. Sugimoto, T. Fukuda, T. Terashima, A. H. Nevidomskyy, et al., Nature **486**, 382 (2012).
[19] E. Thewalt, I. M. Hayes, J. P. Hinton, A. Little, S. Patankar, L. Wu, T. Helm, C. V. Stan, N. Tamura, J. G. Analytis, et al., Phys. Rev. Lett. **121**, 027001 (2018).
[20] T. Iye, M.-H. Julien, H. Mayaffre, M. Horvatić, C. Berthier, K. Ishida, H. Ikeda, S. Kasahara, T. Shibauchi, and Y. Matsuda, Journal of the Physical Society of Japan **84**, 043705 (2015).
[21] E. P. Rosenthal, E. F. Andrade, C. J. Arguello, R. M. Fernandes, L. Y. Xing, X. C. Wang, C. Q. Jin, A. J. Millis, and A. N. Pasupathy, Nature Physics **10**, 225 (2014), ISSN 1745-2481.
[22] H. Man, X. Lu, J. S. Chen, R. Zhang, W. Zhang, H. Luo, J. Kulda, A. Ivanov, T. Keller, E. Morosan, et al., Phys. Rev. B **92**, 134521 (2015).
[23] K. W. Song and A. E. Koshelev, Phys. Rev. B **94**, 094509 (2016).
[24] L. Stojchevska, T. Mertelj, J.-H. Chu, I. R. Fisher, and D. Mihailovic, Phys. Rev. B **86**, 024519 (2012).
[25] T. Shimojima, T. Sonobe, W. Malaeb, K. Shinada, A. Chainani, S. Shin, T. Yoshida, S. Ideta, A. Fujimori, H. Kumigashira, et al., Phys. Rev. B **89**, 045101 (2014).
[26] T. Sonobe, T. Shimojima, A. Nakamura, M. Nakajima, S. Uchida, K. Kihou, C. H. Lee, A. Iyo, H. Eisaki, K. Ohgushi, et al., Scientific Reports **8**, 2169 (2018).
[27] P. Zhang, T. Qian, P. Richard, X. P. Wang, H. Miao, B. Q. Lv, B. B. Fu, T. Wolf, C. Meingast, X. X. Wu, et al., Phys. Rev. B **91**, 214503 (2015).
[28] M. Toyoda, Y. Kobayashi, and M. Itoh, Phys. Rev. B **97**, 094515 (2018).
[29] P. Wiecki, M. Nandi, A. E. Böhmer, S. L. Bud'ko, P. C. Canfield, and Y. Furukawa, Phys. Rev. B **96**, 180502 (2017).
[30] Y. Yuan, X. Fan, X. Wang, K. He, Y. Zhang, Q.-K. Xue, and W. Li, Nature Communications **12**, 2196 (2021).
[31] W. Li, Y. Zhang, P. Deng, Z. Xu, S.-K. Mo, M. Yi, H. Ding, M. Hashimoto, R. G. Moore, D.-H. Lu, et al., Nature Physics **13**, 957 (2017).
[32] C. M. Yim, C. Trainer, R. Aluru, S. Chi, W. N. Hardy, R. Liang, D. Bonn, and P. Wahl, Nature Communications **9**, 2602 (2018).
[33] T. Shimojima, Y. Motoyui, T. Taniuchi, C. Bareille, S. Onari, H. Kontani, M. Nakajima, S. Kasahara, T. Shibauchi, Y. Matsuda, et al., Science **373**, 1122 (2021).
[34] X. Luo, V. Stanev, B. Shen, L. Fang, X. S. Ling, R. Osborn, S. Rosenkranz, T. M. Benseman, R. Divan, W.-K. Kwok, et al., Phys. Rev. B **91**, 094512 (2015).
[35] J. Cardy, *Scaling and Renormalization in Statistical Physics* (Cambridge University Press, 1996).
[36] K. W. Song and A. E. Koshelev, Phys. Rev. B **94**, 094509 (2016).
[37] R. M. Fernandes, L. H. VanBebber, S. Bhattacharya, P. Chandra, V. Keppens, D. Mandrus, M. A. McGuire, B. C. Sales, A. S. Sefat, and J. Schmalian, Phys. Rev.

Lett. **105**, 157003 (2010).
[38] T. Goto, R. Kurihara, K. Araki, K. Mitsumoto, M. Akatsu, Y. Nemoto, S. Tatematsu, and M. Sato, Journal of the Physical Society of Japan **80**, 073702 (2011).
[39] M. Yoshizawa, D. Kimura, T. Chiba, S. Simayi, Y. Nakanishi, K. Kihou, C.-H. Lee, A. Iyo, H. Eisaki, M. Nakajima, et al., Journal of the Physical Society of Japan **81**, 024604 (2012).
[40] R. M. Fernandes, A. E. Böhmer, C. Meingast, and J. Schmalian, Phys. Rev. Lett. **111**, 137001 (2013).
[41] A. M. Merritt, F. Weber, J.-P. Castellan, T. Wolf, D. Ishikawa, A. H. Said, A. Alatas, R. M. Fernandes, A. Q. R. Baron, and D. Reznik, Phys. Rev. Lett. **124**, 157001 (2020).
[42] S. Chibani, D. Farina, P. Massat, M. Cazayous, A. Sacuto, T. Urata, Y. Tanabe, K. Tanigaki, A. E. Böhmer, P. C. Canfield, et al., npj Quantum Materials **6**, 37 (2021).
[43] Y. Qi and C. Xu, Phys. Rev. B **80**, 094402 (2009).
[44] U. Karahasanovic and J. Schmalian, Phys. Rev. B **93**, 064520 (2016).
[45] I. Paul and M. Garst, Phys. Rev. Lett. **118**, 227601 (2017).
[46] V. S. de Carvalho and R. M. Fernandes, Phys. Rev. B **100**, 115103 (2019).
[47] E. W. Carlson, K. A. Dahmen, E. Fradkin, and S. A. Kivelson, Phys. Rev. Lett. **96**, 097003 (2006).
[48] H.-H. Kuo, J.-H. Chu, J. C. Palmstrom, S. A. Kivelson, and I. R. Fisher, Science **352**, 958 (2016).
[49] P. Wiecki, R. Zhou, M.-H. Julien, A. E. Böhmer, and J. Schmalian, Phys. Rev. B **104**, 125134 (2021).
[50] A. Lahiri, Master's thesis, University of Minnesota (2021).
[51] E. Lifshitz, A. Kosevich, and L. Pitaevskii, *Theory of Elasticity* (Butterworth-Heinemann, 1986).
[52] L. Nie, G. Tarjus, and S. A. Kivelson, Proceedings of the National Academy of Sciences **111**, 7980 (2014).
[53] T. Cui and R. M. Fernandes, Phys. Rev. B **98**, 085117 (2018).
[54] V. Marchenko and A. Y. Parshin, JETP Lett. **52**, 129 (1980), [ZhETF, Vol. 79, No. 1, p. 257, July 1980].
[55] L. E. Shilkrot and D. J. Srolovitz, Phys. Rev. B **53**, 11120 (1996).
[56] J. Stewart, O. Pohland, and J. M. Gibson, Phys. Rev. B **49**, 13848 (1994).
[57] *Point Defects* (John Wiley & Sons, Ltd, 2005), ISBN 9783527606672.
[58] D. Bacon, D. Barnett, and R. Scattergood, Progress in Materials Science **23**, 51 (1980).
[59] E. Clouet, C. Varvenne, and T. Jourdan, Computational Materials Science **147**, 49 (2018).
[60] C. Teodosiu, *Elastic Models of Crystal Defects* (Springer-Verlag, 1982), 1st ed.
[61] See Supplemental Material at [URL will be inserted by publisher] for details of the defect-induced nematic potential for both step and generic point defects, the derivation of the smectic critical temperature, the eventual surface smectic to uniform bulk nematic transition, and comparison with the PEEM data of T. Shimojima et al, Science **373**, 1122, (2021).
[62] C. De Dominicis and I. Giardina, *Random Fields and Spin Glasses: A Field Theory Approach* (Cambridge University Press, 2006).
[63] V. Dotsenko, *Introduction to the Replica Theory of Disordered Statistical Systems*, Collection Alea-Saclay: Monographs and Texts in Statistical Physics (Cambridge University Press, 2000).
[64] Y. Imry and S.-k. Ma, Phys. Rev. Lett. **35**, 1399 (1975).
[65] A. Aharony, Y. Imry, and S.-k. Ma, Phys. Rev. Lett. **37**, 1364 (1976).
[66] G. Grinstein, Phys. Rev. Lett. **37**, 944 (1976).
[67] M. Mézard and A. P. Young, Europhysics Letters (EPL) **18**, 653 (1992).
[68] A. P. Young, Journal of Physics C: Solid State Physics **10**, L257 (1977).
[69] S. Hameed, D. Pelc, Z. W. Anderson, A. Klein, R. J. Spieker, L. Yue, B. Das, J. Ramberger, M. Lukas, Y. Liu, et al., Nature Materials (2021).
[70] R. Willa, M. Hecker, R. M. Fernandes, and J. Schmalian, Phys. Rev. B **104**, 024511 (2021).
[71] S. Avci, O. Chmaissem, D. Y. Chung, S. Rosenkranz, E. A. Goremychkin, J. P. Castellan, I. S. Todorov, J. A. Schlueter, H. Claus, A. Daoud-Aladine, et al., Phys. Rev. B **85**, 184507 (2012).
[72] H. Murayama, Y. Sato, R. Kurihara, S. Kasahara, Y. Mizukami, Y. Kasahara, H. Uchiyama, A. Yamamoto, E.-G. Moon, J. Cai, et al., Nature Communications **10**, 3282 (2019).
[73] T. Shimojima, *Data for science paper 2021* (2021), URL https://doi.org/10.5281/zenodo.4885407.
[74] A. Klein, M. H. Christensen, and R. M. Fernandes, Phys. Rev. Research **2**, 013336 (2020).
[75] P. Reiss, M. D. Watson, T. K. Kim, A. A. Haghighirad, D. N. Woodruff, M. Bruma, S. J. Clarke, and A. I. Coldea, Phys. Rev. B **96**, 121103 (2017).
[76] S. Chandra and A. Islam, Physica C: Superconductivity **470**, 2072 (2010), ISSN 0921-4534.
[77] V. Brouet, M. F. Jensen, P.-H. Lin, A. Taleb-Ibrahimi, P. Le Fèvre, F. Bertran, C.-H. Lin, W. Ku, A. Forget, and D. Colson, Phys. Rev. B **86**, 075123 (2012).
[78] L. E. Shilkrot and D. J. Srolovitz, Phys. Rev. B **55**, 4737 (1997).
[79] P. Müller and A. Saúl, Surface Science Reports **54**, 157 (2004).